

Angular distributions of multiphoton detachment of H^- in various infrared laser fields

Lihua Bai,^{1,2} Jingtao Zhang,^{1,*} Xiaoming Zhang,³ and Zhizhan Xu^{1,3,†}

¹State Key Laboratory of High Field Laser Physics, Shanghai Institute of Optics and Fine Mechanics, Chinese Academy of Sciences, Shanghai 201800, China

²Graduate School of Chinese Academy of Sciences, Beijing 100049, China

³State Key Laboratory for Mesoscopic Physics, Department of Physics, Peking University, Beijing 100087, China

(Received 22 January 2006; revised manuscript received 25 July 2006; published 31 August 2006)

Using a nonperturbative quantum scattering theory, the photoelectron angular distributions (PADs) from the multiphoton detachment of H^- ions in strong, linearly polarized infrared laser fields are obtained to interpret recent experimental observations. In our theoretical treatment, the PADs in n -photon detachment are determined by the n th-order generalized phased Bessel (GPB) functions $\mathcal{X}_{-n}(Z_f, \eta)$. The advantage of using the GPB scenario to calculate PADs is its simplicity: a single special function (GPB) without any mixing coefficient can express PADs observed by recent experiments. Thus, the GPB scenario can be called a parameterless scenario.

DOI: [10.1103/PhysRevA.74.025402](https://doi.org/10.1103/PhysRevA.74.025402)

PACS number(s): 32.80.Rm, 42.65.Ky, 12.20.Ds, 03.65.Nk

Recently, more and more interests has arisen in the study of multiphoton detachment of H^- both experimentally [1–4] and theoretically [5–10]. To interpret an experiment [1], Telnov and Chu, in a theoretical study by means of a Floquet treatment [8], reproduced the photoelectron angular distributions (PADs) from the detachment of H^- which had the main feature of the experiment measurement: the two-photon PADs exhibited a structure containing a pair of main lobes and a central jet. Here, the words “main lobe” mean the formation of the detached photoelectrons around the direction of laser polarization, while the “jet” means a peaked-out formation of photoelectrons emitted from the waist between the two main lobes [11]. Telnov and Chu treated H^- as an accurate one-electron model [6,8], and expanded the detachment rate in terms of Legendre polynomials with combination coefficients. They interpreted their treatment as a partial-wave mixing or quantum interference.

The nonperturbative scattering theory for multiphoton ionization (MPI) in intense fields derived by Guo, Åberg, and Crasemann (GAC) [12] has had a notable success in an explanation of the strong-field phenomena, such as the angular distribution splitting observed by Bucksbaum *et al.* [13,14] and the recent observation of the jetlike structure in PADs by Nandor *et al.* [11,15]. This theory shows: (1) the PADs are uniquely determined by the generalized phased Bessel (GPB) function; (2) the jets feature the maxima of the generalized phased Bessel function and the number of jets follows the number rule derived by the theory; and (3) all PADs in different laser frequencies, laser intensities, and atomic binding energies are related by a scaling law [16]. In this Brief Report, we show the application of GAC theory to the study of the laser intensity and wavelength dependence of PADs of the two- and many-photon detachment of H^- . We show that the ratio of the height of the central jet to that of the main lobe varies with the laser intensity and the laser wavelength. With increasing the laser intensity in a fixed

laser wavelength, the height of the central jet becomes larger and larger, while the main lobe becomes smaller and smaller, eventually the central jet becomes dominant in PADs. The advantage of using the GAC theory to interpret PADs lies in its simplicity and ability to reproduce PAD patterns observed by experiments. In the GAC theory, the PADs are described by a single special function, not a superposition of a set of special functions. Thus, the interpretation of the experimental result made by this theory can be said to be a “parameterless interpretation.”

The differential detachment-rate formula is given by [12,17]

$$\left. \frac{d^2W}{d^2\Omega_{\mathbf{P}_f}} \right|_j = \frac{e^2\omega^{9/2}}{(2m_e)^{1/2}(2\pi)^5} (j - \epsilon_b - u_p)^{1/2} (j - u_p)^2 \times \sum_{q > \epsilon_b} (u_p - j + q) \int d^2\Omega_{\mathbf{k}'} |\Phi_i(\mathbf{P}_f - q\mathbf{k} + \mathbf{k}')|^2 |\mathcal{X}_q|^2, \quad (1)$$

where $d\Omega_{\mathbf{P}_f}$ is the differential solid angle in the space of the final photoelectron momentum \mathbf{P}_f ; j is the number of the absorbed photons in the detachment process; \mathbf{k} and \mathbf{k}' are wave vectors of the laser field and the spontaneously emitted light, respectively; $\epsilon_b = E_b/\omega$ is the atomic binding energy per laser-photon energy and the ponderomotive parameter $u_p \equiv U_p/\omega$; $\Phi_i(\mathbf{P})$ is the Fourier transform of the initial wave function. The function $\mathcal{X}_q(\mathbf{P}_f, \mathbf{k}')$ is defined as

$$\mathcal{X}_q = \frac{\mathcal{X}_{-j}(Z, \eta)}{\omega} \sum_{j'=-\infty}^{\infty} \frac{\mathcal{X}_{-j'}(Z, \eta)}{u_p - j'} \{ -\mathbf{P}'_f \cdot \boldsymbol{\epsilon}'^* X_{q-j+j'}(Z_{k'}) + e\Lambda \boldsymbol{\epsilon}'^* \cdot [\boldsymbol{\epsilon}'^* X_{q-j+j'+1}(Z_{k'}) + \boldsymbol{\epsilon} X_{q-j+j'-1}(Z_{k'})] \}, \quad (2)$$

and $\mathbf{P}'_f = \mathbf{P}_f + (j - q - u_p)\mathbf{k}$, the generalized phased Bessel (GPB) function

*Corresponding author. Email address: jtzhang@siom.ac.cn

†Corresponding author. Email address: zzzxu@mail.shnc.ac.cn

$$\mathcal{X}_{-j}(Z, \eta) = \sum_{s=-\infty}^{\infty} X_{-j+2s}(Z)X_{-s}(\eta) \quad (3)$$

is defined by the phased Bessel function $X_n(Z)$, which relates to the ordinary Bessel function as $X_n(Z) = J_n(|Z|)e^{in\arg(Z)}$. The complex arguments of the generalized phased Bessel function are, $Z_f = 2\sqrt{u_p/m_e\omega}\mathbf{P}_f \cdot \boldsymbol{\epsilon}$, $Z_{k'} = 2\sqrt{u_p/m_e\omega}\mathbf{k}' \cdot \boldsymbol{\epsilon}$, $Z = Z_f + Z_{k'}$, and $\eta = (1/2)u_p$. In Eq. (2), $\boldsymbol{\epsilon}$ and $\boldsymbol{\epsilon}'$ are the polarization vectors of the laser light and the spontaneous emission, respectively. In the long-wavelength approximation, $Z_{k'} \ll Z_f$, which leads to $Z \approx Z_f$. These notations agree with Ref. [15].

Our calculated PADs are obtained, according to Eq. (1), by fixing the scattering angle at $\pi/2$ and varying the azimuthal angle from 0° and 180° with the step size of 6° . In our calculations, the binding energy is chosen as 0.75421 eV [18]. The initial wave function is chosen as the ground-state wave function of H^- suggested by Armstrong [19]. Our calculated PADs in linearly polarized laser fields, as in the partial-mixing theory, also show rich structures; besides the main lobes around the direction of laser polarization, prominent electron “jets” are emitted from the waist between the two main lobes. In the following, we first discuss the laser-wavelength dependence and the laser-intensity dependence of PADs using the two-photon detachment as an example, then, we extend the discussion to many-photon detachments. In the PADs of the two-photon detachment, there is always the central jet. The ratio of the height of the central jet to that of the main lobe varies with the laser intensity and the laser frequency. With this ratio, we study the laser intensity and wavelength dependence of PADs.

The laser-wavelength dependence of PADs. The laser-wavelength dependence of PADs can be in many aspects. For example, the PADs and the electron kinetic spectrum vary with the laser frequency [20]. If the laser frequency varies in a large domain, the number of the absorbed photons in the detachment process will be changed, and the PADs will show dramatic change. Focusing on the two-photon detachment of H^- ions, we choose the laser wavelength varying from 1.8 to $2.7 \mu\text{m}$, correspondingly, the photon energy varies from 0.69 to 0.46 eV. Thus, two photons are absorbed to form the first detachment peak.

We first show the calculated PADs at a relatively low laser intensity, e.g., $1 \times 10^{10} \text{ W/cm}^2$, in Fig. 1. The PADs corresponding to four different wavelengths are depicted. Each of the plots in Fig. 1 shows the main lobe around the laser polarization and the central jet perpendicular to the laser polarization, but the ratio of the height of the jet to that of the main lobe varies with the laser wavelength. In plot (a), which is for laser wavelength $\lambda = 1.8 \mu\text{m}$, the height of the main lobe is much higher than that of the central jet, and the ratio is larger than 6.0 . With increasing the laser wavelength, the central jet becomes bigger and bigger, as shown in plot (b) for $\lambda = 2.1 \mu\text{m}$ and in plot (c) for $\lambda = 2.4 \mu\text{m}$. For the PAD with $\lambda = 2.7 \mu\text{m}$ shown in plot (d), the central jet becomes dominant, such that the detached electrons are ejected mostly perpendicularly to the laser polarization. This is the so-called threshold effect by Reichle *et al.* [1] and also theoretically obtained by means of the Floquet calculation [6]. Our calcu-

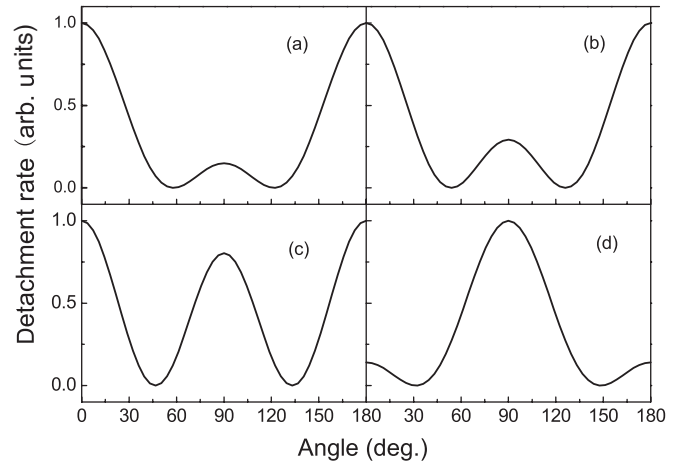


FIG. 1. Electron angular distributions after the two-photon detachment of H^- for a fixed laser intensity $1 \times 10^{10} \text{ W/cm}^2$ at different central laser wavelengths (a) $1.8 \mu\text{m}$, (b) $2.1 \mu\text{m}$, (c) $2.4 \mu\text{m}$, and (d) $2.7 \mu\text{m}$. For the convenience of comparison, each plot is normalized by the maximum of PAD.

lations show that this effect originates from the geometric property of the GPB function $\mathcal{X}_{-2}(Z, \eta)$. At higher intensities, this effect is even more evident. We show in Fig. 2 the PADs for a higher laser intensity $2 \times 10^{11} \text{ W/cm}^2$. At this intensity, the height of the central jet, compared with the corresponding one in Fig. 1, has more drastic changes with the wavelength. The central jet becomes dominant in plot (c) and in plot (d), the main lobe disappears and the PAD just shows a large central jet.

The laser-intensity dependence of PADs. The laser intensity affects the detachment rate and the distribution of the ejected electrons. Our calculations show that the PADs of a two-photon detachment in laser fields of lower intensity and lower frequency are similar to those in laser fields of higher intensity and higher frequency, as shown in Figs. 1 and 2. For example, PAD in Fig. 1(b) is similar to that in Fig. 2(a). Here, we focus on the laser-intensity dependence of the PADs of the two-photon detachment. To ensure that the calculated detachment occurs with absorption of two photons

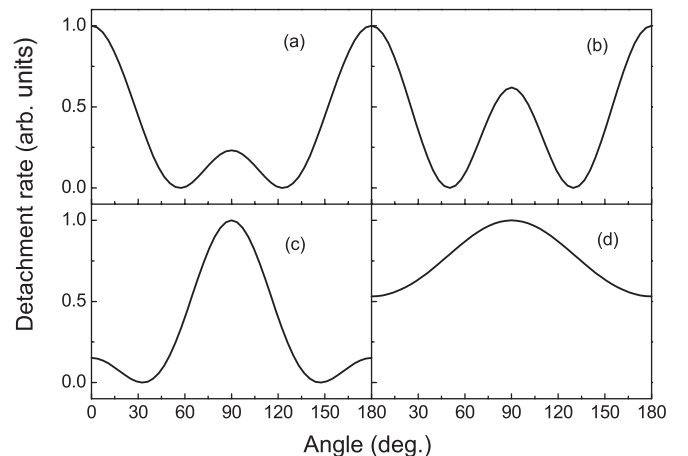


FIG. 2. The same as that in Fig. 1, but for laser intensity $2 \times 10^{11} \text{ W/cm}^2$.

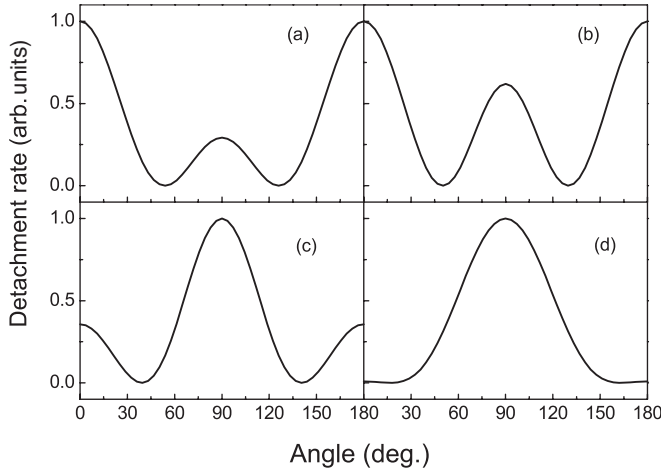


FIG. 3. Electron angular distributions after the two-photon detachment of H^- at different laser intensities, (a) 1×10^{10} W/cm 2 , (b) 2×10^{11} W/cm 2 , (c) 5×10^{11} W/cm 2 , and (d) 7×10^{11} W/cm 2 . The central wavelength of the laser field is chosen as $2.1 \mu\text{m}$.

(with wavelength $2.1 \mu\text{m}$), we choose the laser intensity varying from zero to a maximum 1×10^{12} W/cm 2 . Figure 3 shows the calculated PADs of the two-photon detachment at several laser intensities, by which the dependence on the laser intensity is clear. The PADs show a main lobe and a central jet. The laser-intensity dependence of PADs is described by the ratio of the height of the central jet to that of the main lobe. When the laser intensity is less than 1×10^{11} W/cm 2 , the central jet in the PADs shows no distinct change, and most calculated PADs are similar to the one shown in plot (a) for laser intensity 1×10^{11} W/cm 2 . With increasing laser intensities, the central jet becomes larger and larger, as shown in plot (b) for laser intensity 2×10^{11} W/cm 2 . The central jet finally exceeds the main lobe, as shown in plot (c) for laser intensity 5×10^{11} W/cm 2 . The main lobe becomes smaller and smaller with increasing laser intensity, and finally disappears. Then the PAD just exhibits a large central jet, as shown in plot (d) for laser intensity 7×10^{11} W/cm 2 . The central jet broadens more and more with increasing laser intensities, and eventually becomes flat. The flat line, which corresponds to an isotropic distribution of the detached electrons, means that the two-photon detachment channel will be closed if the laser intensity is further increased.

PADs in many-photon detachments and their parity property. The PADs of other higher-order detachment channels from our calculation also show good agreement with the experimental observations. More jets appear in the PADs of the higher-order detachments. There is a central jet in a four-photon PAD, but no central jet in any PAD of odd-photon detachment. For the incident laser field of the wavelength $2.15 \mu\text{m}$ and the intensity 3×10^{11} W/cm 2 , the calculated PADs (not shown here) look quite similar to those obtained with the superpositions of Legendre polynomials (see Fig. 9 of Ref. [21]). In our calculated PADs of a three-photon detachment, two side jets stick out clearly at azimuthal angles $\phi_f = 60^\circ, 120^\circ$, respectively, as well as the opposite direction. The side jets in the three-photon detachment, in the solid

angle of the momentum space, form the winglike structure in Fig. 3 of Ref. [1]. The experimentally measured data in the three-photon case support our no-central-jet conclusion. For other higher-order detachment channels, because the height of the jets is much lower, the jets submerge in the blue background in Fig. 3 of Ref. [1]. In general, our theory confirms the observation of Reichle *et al.*

Using partial-wave expansion, i.e., the Legendre polynomial expansion to express the electron scattering state is a traditional method from perturbative quantum mechanics. A great advantage of doing so is that all the partial waves have their parity property. A single electric (dipole) photon possesses an odd parity; a pure (or mixed) atomic angular momentum state can be expressed by a single (or a combination of) Legendre polynomial(s). The parity conservation law strictly governs all electromagnetic processes. With the partial-wave expansion, the parity conservation can be guaranteed and easily tracked. Our GPB scenario has the same advantage in guaranteeing and tracking the parity conservation as the partial-wave scenario does but with the parameterless feature. In the GPB scenario, the PADs for an n -photon detachment are determined by the n th-order GPB function $\mathcal{X}_{-n}(Z_f, \eta)$, which has the parity property: $\mathcal{X}_{-n}(-Z_f, \eta) = (-1)^n \mathcal{X}_{-n}(Z_f, \eta)$, which shows that the odd-order GPB functions are odd functions of the first variable and the even-order GPB functions are even functions. An odd function vanishes at the origin, corresponding to no central jet in a PAD. All even-order GPB functions have nonvanishing value at the origin as a half maximum [15], thus, show the central jet in PADs. Since the order of a GPB function signifies the transferred photon numbers, in a transition process with transferring an even or odd number of photons, the GPB will automatically take the parity conservation into account. The ratio of the height of the central jet to that of the main lobe is determined by the value of $|\mathcal{X}_{-2n}(0, \eta)| / |\mathcal{X}_{-2n}(Z_{f\text{max}}, \eta)|$, where $|\mathcal{X}_{-2n}(0, \eta)| = |\mathcal{X}_{-n}(\eta)|$ denotes the amplitude of the central jet in PADs while $|\mathcal{X}_{-2n}(Z_{f\text{max}}, \eta)|$ corresponds to the detachment-rate amplitude in the laser polarization. Because $Z_{f\text{max}}$ and η vary with the laser intensity and the laser frequency, the laser-intensity and the laser-frequency dependence of PADs can be manifested by the variation of height ratio of the central jet versus the main lobe.

The laser-intensity and the laser-frequency dependence of PADs are through the variation of $u_p = 2\pi e^2 I / m_e \omega^3$ with the laser intensity and the laser frequency. A higher laser intensity and/or a lower laser frequency correspond to a larger ponderomotive shift. The energy conservation in the overall process determines the final kinetic energy of the electron after the n -photon detachment, satisfying $E_k \equiv \mathbf{P}_f^2 / 2m_e = n\omega - u_p \omega - E_b$, which leads to a decrease in the final kinetic energy with increasing laser intensity and/or decreasing laser frequency. Thus, the PADs vary with laser intensities and laser frequencies.

In the following, we use the two-photon detachment as an example to show the physical meaning. The variables of the GPB function describing the photoelectron after the n -photon detachment can be written as $Z_f = \sqrt{8u_p(n - u_p - \epsilon_b)} \cos \phi_f = Z_{f\text{max}} \cos \phi_f$. The corresponding value of Z_f that leads to

$\mathcal{X}_{-2}(Z_f, \eta)=0$, which is the first zero point for the GPB function, can be denoted by Z_{f0} . With the change of the laser intensity and/or the laser frequency, u_p changes, as well as the values of $Z_{f\max}$ and η , which leads to changes of Z_{f0} and the ratio of $|\mathcal{X}_{-2}(0, \eta)|/|\mathcal{X}_{-2}(Z_{f\max}, \eta)|$. These changes show the laser-wavelength and the laser-intensity dependence of the PADs.

At each fixed laser intensity, as shown in Figs. 1 and 2, the increasing of the laser wavelength enlarges the ponderomotive shift, which leads to two changes in the GPB function; the value of $Z_{f\max}$ changes and the value of Z_{f0} becomes larger. These changes increase the value of $|\mathcal{X}_{-2}(0, \eta)|/|\mathcal{X}_{-2}(Z_{f\max}, \eta)|$. Correspondingly, the central jet in PADs gets bigger and bigger with increasing laser wavelength. If the laser wavelength is large enough so that $Z_{f0} > Z_{f\max}$, the main lobe will disappear and there exists just a large jet in (one side of) the PADs.

At fixed laser wavelengths, the ponderomotive shift is only determined by the laser intensity. In a relatively low-intensity regime, u_p is small. Thus the two variables of the GPB function are very small and their variation with the laser intensity is not distinct. Correspondingly, the variation of the PADs in the lower-intensity regime is not distinct. This is why the PADs do not show obvious change until the laser intensity is higher than 1×10^{11} W/cm². With increasing the laser intensity, u_p becomes notable, the value of $Z_{f\max}$ becomes small, and that of Z_{f0} gets large. Correspondingly, the

jet gets bigger and bigger. At some intensity, $Z_{f\max} < Z_{f0}$, the main lobe in the PADs disappears, and there exists only one big jet in one side of the PAD. The value of $Z_{f\max}$ becomes even smaller with further increasing laser intensities, and the jet becomes broader and broader. There is a critical intensity limit near $n\omega - (u_p\omega + E_b) = 0^+$, as well as $n=2$; beyond this limit (0^-) the n -photon (or the 2-photon) channel will be suppressed, the value of $Z_{f\max}$ tends to zero, and the value of $|\mathcal{X}_{-2n}(0, \eta)| = X_{-n}(\eta)$ shows no change with the azimuth. Thus the PAD becomes isotropic.

Summary. The n -photon PADs are determined by the n th-order GPB function $\mathcal{X}_{-n}(Z_f, \eta)$; the main lobes of PADs are along the laser polarized direction and a central jet occurs perpendicular to the polarized direction for the even-photon detachment. The central jet in the PADs manifests the non-vanishing value of this even GPB function at the origin as a half maximum. The advantage of this treatment is its simplicity. A single special function (GPB) without any mixing coefficient can express PADs observed by recent experiments.

This work is supported by the Shanghai Rising-Star Program, the Chinese National Natural Science Foundation under Grant No. 60408008, and the Natural Science Key Foundation of Shanghai under Grant No. 04JC14036. We are grateful to Professor D.-S. Guo for his great help in this paper.

-
- [1] R. Reichle, H. Helm, and I. Y. Kiyani, Phys. Rev. Lett. **87**, 243001 (2001).
- [2] W. W. Smith *et al.*, J. Opt. Soc. Am. B **8**, 17 (1991).
- [3] C. Y. Tang *et al.*, Phys. Rev. Lett. **66**, 3124 (1991).
- [4] C. Y. Tang *et al.*, Phys. Rev. A **39**, 6068 (1989).
- [5] S. Geltman, Phys. Rev. A **43**, 4930 (1991).
- [6] D. A. Telnov and Shih-I Chu, Phys. Rev. A **66**, 063409 (2002).
- [7] D. A. Telnov and Shih-I Chu, J. Phys. B **29**, 4401 (1996).
- [8] C. Laughlin and Shih-I Chu, Phys. Rev. A **48**, 4654 (1993).
- [9] J. Wang, Shih-I Chu, and C. Laughlin, Phys. Rev. A **50**, 3208 (1994).
- [10] D. A. Telnov and Shih-I Chu, Phys. Rev. A **59**, 2864 (1999).
- [11] M. J. Nandor, M. A. Walker, and L. D. Van Woerkom, J. Phys. B **31**, 4617 (1998).
- [12] D.-S. Guo, T. Aberg, and B. Crasemann, Phys. Rev. A **40**, 4997 (1989).
- [13] D.-S. Guo and G. W. F. Drake, Phys. Rev. A **45**, 6622 (1992).
- [14] P. H. Bucksbaum, D. W. Schumacher, and M. Bashkansky, Phys. Rev. Lett. **61**, 1182 (1988).
- [15] Jingtao Zhang *et al.*, J. Phys. B **35**, 4809 (2002).
- [16] D.-S. Guo *et al.*, Phys. Rev. A **68**, 043404 (2003).
- [17] J. Gao, D.-S. Guo, and Y. S. Wu, Phys. Rev. A **61**, 043406 (2000).
- [18] T. Andersen, H. K. Haugen, and K. Hotop, J. Phys. Chem. Ref. Data **28**, 1511 (1999).
- [19] B. H. Armstrong, Phys. Rev. **131**, 1132 (1963).
- [20] P. Kaminski *et al.*, Phys. Rev. A **70**, 053413 (2004).
- [21] R. Reichle, H. Helm, and I. Y. Kiyani, Phys. Rev. A **68**, 063404 (2003).